Available online at www.sciencedirect.com
ScienceDirect
Journal of Power Sources 162 (2006) 521–531
JOURNAL OF POWER SOURCES
www.elsevier.com/locate/jpowsour

Durability study of proton exchange membrane fuel cells under dynamic testing conditions with cyclic current profile

D. Liu [a], S. Case [b,*]

[a] *Macromolecular Science and Engineering, Virginia Polytechnic Institute and State University, Blacksburg, VA 24061, USA*
[b] *Engineering Science and Mechanics, Virginia Polytechnic Institute and State University, Blacksburg, VA 24061, USA*

Received 6 June 2006; received in revised form 3 July 2006; accepted 4 July 2006
Available online 14 August 2006

Abstract

This work addresses issues of long-term durability of hydrogen–air proton exchange membrane fuel cells (PEMFCs) under cyclic current loading conditions, simulating the real road driving conditions for automotives. The same type of membrane–electrode assembly (MEA) was also aged under constant current mode as a control and the results were compared with those of the cyclically aged MEA. Both MEAs were characterized for cell polarizations, impedance spectra, Tafel plots, hydrogen crossover rates as well as electrochemical active surface areas at intervals of 100 h of aging. It was demonstrated that hydrogen crossover increased dramatically after 500 h of current cycling due to pinhole formation and was the most dominant degradation source. The fuel cell approached the end of its useful lifetime after 1000 h of operation. On the other hand, the hydrogen crossover rate remained approximately constant for the MEA under constant current operation. Mass transport limitations were identified as the major source of decreased performance during the constant current operation. This decrease in performance was partially reversible when cathode flooding was resolved by setting the cell at lower current densities. At the end, a phenomenological durability model was established successfully to describe the aging processes and cell performance at different time nodes.

Keywords: Proton exchange membrane fuel cell; Durability; Cyclic current mode; Aging diagnosis; Phenomenological modeling

1. Introduction

Durability studies of proton exchange membrane fuel cells (PEMFCs) have attracted enormous attention for the last 3 years. A great deal of research effort has been devoted to meeting the Department of Energy (DOE) targets, such as 5000 h of operational lifetime for PEMFC stacks in automotive applications [1]. There are two stages associated with the durability studies of PEMFCs. In the first stage, the degradation sources and mechanisms of PEMFC components/system are identified, with respect to different system configurations, various material selections, and different operation conditions. Experimental observations are conducted to characterize the aging phenomena as functions of time. In the second stage, mathematical models are developed to predict the degradations in a PEMFC system, in which expressions of the aging phenomena and aging effects are incorporated into performance models through constitutive relations. For the durability model to achieve good accuracy and maximum predictive power, multi-dimensional microscopic modeling based on the classic conservation laws is required, leading to great complexity. As an intermediate step, a phenomenological model with values of aging parameters substituted into the semi-empirical fuel cell performance equations at different time nodes can be employed to begin the durability modeling process. But in the literature, the durability study of PEMFCs remains in the first stage, with mostly experimental characterizations presented [2].

As is known, the operation conditions associated with PEMFCs include a strong acidic environment (pH ∼ 2), oxygen in gaseous phase and dissolved phase, water in vapor and liquid phase, tensile/compressive stresses, contamination, cyclic temperature and dynamic load cycles. The associated aging processes may occur in the polymer membrane, catalyst layers, electrodes, membrane–catalyst interface, monopolar/bipolar plates, sealing materials and current collectors. Ref. [2] provides a nice summary of the reported degradation sources from PEMFC components. Long-term aging studies were also conducted to

* Corresponding author. Tel.: +1 540 231 3140; fax: +1 540 231 9187.
E-mail address: scase@exchange.vt.edu (S. Case).

0378-7753/$ – see front matter © 2006 Elsevier B.V. All rights reserved.
doi:10.1016/j.jpowsour.2006.07.007

investigate the effects of operation conditions on fuel cell durability [2–5].

St-Pierre et al. at Ballard Power Systems performed a series of aging tests for PEMFC stacks (primarily MK5 and MK513 stacks) under different operating conditions [5]. The effects of water management with high and low humidification levels, contamination, pressure, temperature and reactant stoichiometry were inspected with the introduction of possible mitigating strategies. They concluded that poor water management could cause PEMFC performance degradation due to mass transport limitations. Counterflow patterns in the bipolar plates, temperature gradients, changes in substrate hygrophobicity and load cycling were examined to help reduce the mass transport issues. In addition, the influence of freeze-thaw cycles was examined. These cycles showed insignificant degradations in PEMFC performance after 55 cycles.

Recently, Xie et al. carried out a long-term durability study of hydrogen–air PEM fuel cells. Two types of MEAs were investigated under constant current mode with different current settings and high humidity level for 2000 h [6]. Characterizations of the aged MEAs were performed periodically, including voltage decay, polarization, electrochemical active surface (EAS) area, and fluoride ion and catalyst metallic concentration in cathode exhaust water. The result revealed that one type of metal particles in the catalyst alloy migrated from cathode to anode during the aging process, reducing the EAS area. Scanning and transmission electron images of MEA cross-sections after aging showed the loss of carbon-supported catalyst clusters and possible dissolution of recast Nafion ionomer. Fluoride and sulfate anions were detected in the cathode outlet water by high performance liquid chromatography (HPLC)-mass spectrometry (MS) technique, proving the degradation/dissolution of ionomers.

The paper by Xie et al. presented a comprehensive list of characterizations for PEMFCs after aging. Nevertheless, they inspected the MEA performances under constant current mode, which is different from the real road driving scenario. The degradations of cell components may vary with respect to the current/power output spectrum. Wilkinson and St-Pierre examined the dynamic operation of 8-cell and 20-cell PEMFC stacks with modified urban transit authority (UMTA) driving cycles [2]. Small performance degradation was demonstrated for these stacks over 5000 h; most of the performance loss was found to be reversible. They did not provide detailed diagnosis for sources of the degradation in their report. Neither were the impacts of urban driving cycles on the PEMFC material and system deterioration identified.

In this article, the aging mechanisms of the same type of commercially available hydrogen–air MEAs were characterized under cyclic and constant current loading conditions. Both MEAs were aged for 1000 h in total and diagnosed every 100 h of operation. A semi-empirical phenomenological model was set up to incorporate the observed aging phenomena and describe the cell performance at different aging times. Distinct degradation mechanisms were illustrated after comparing the results under two different aging modes. These results reinforce the need to conduct systematic inspections of PEMFCs to identify the causes of changes in the cell's long-term performance, which are related to the aging behavior of materials, structure, hardware design and operation conditions. They also point to the need for the establishment of standard PEMFC aging protocols.

2. Experimental

2.1. Materials

Two 5 cm^2 standard hydrogen/air MEAs were purchased [7]. The catalyst loadings of both anode and cathode were 0.5 mg cm^{-2}. Acidified Nafion 112 film was employed as the membrane and ETEK ELAT® carbon cloth was applied as the gas diffusion layers (GDL). The MEAs were tested as-received using Fuel Cell Technologies Inc. (FCT) fuel cell test stations. Standard 5 cm^2 PEMFC fixtures were obtained from FCT, with stainless steel monopolar plates and gold-coated copper current collector plates. The ultrapure hydrogen gas cylinder and breathing air cylinder were attached to the FCT stations to supply fuel and oxidant for fuel cell operations [8]. Ultrapure nitrogen gas was utilized for electrochemical measurements [8].

2.2. Measurements

2.2.1. Aging mode

There were two aging modes applied for the aging processes.

2.2.1.1. Cyclic current aging. The cyclic current spectrum was provided as a preliminary cycling profile for durability testing of PEM fuel cells. One of the two MEAs, denoted as MEA1, was aged by use of this cyclic current profile for a total of 1000 h. Each current aging cycle composed of 16 steps including open circuit, low current settings, intermediate current settings and the highest current setting, the details of which are shown in Table 1. One cycle took approximately 6 min to complete. The MEA1 was aged for 10 aging periods, with 1000 cycles or 100 h per period and characterized for a full set of performance and component parameters after each 100 h aging period.

Table 1
The current cycling profile

Step	Duration (s)	Current density (A cm^{-2})
1	15	0
2	25	0.2
3	20	0.4
4	15	0.05
5	24	0.2
6	20	0.4
7	15	0.05
8	25	0.2
9	20	0.4
10	15	0.05
11	35	0.2
12	20	1.06
13	35	0.86
14	8	0.02
15	35	0.4
16	40	0.05

The MEA1 operation was performed at a cell temperature of 80 °C, anode/cathode temperatures of 80 °C and anode/cathode preheater temperature of 81 °C. Both gas lines were fully humidified. The hydrogen flow rate was 200 standard cubic centimeters per minute (sccm) while the air flow rate was 500 sccm. Both electrodes had a backpressure of 138 kPa (20 psi). The MEA1 was tested using an FCT test station with an EMREL-50A-100W electronic box (denoted as test station #1).

Table 1 describes the test protocol to assess the performance and durability of fuel cells for automotive propulsion applications. The goal of this testing is to assess cell and stack performance against DOE targets. This protocol is proposed by an automotive company but not intended to be comprehensive as there are many issues critical to a vehicular fuel cell (e.g., start/stop). It should be recognized that the cycles specified herein have not been fully validated and correlated with data from systems operated under actual drive cycles. Therefore, durability results from this protocol may not be predictive of lifetime in an actual fuel cell vehicle subjected to actual driving and start/stop cycles.

2.2.1.2. Constant current aging. The constant current aging was conducted on MEA2 at the highest current setting from the cyclic aging spectrum (1.06 A cm^{-2}). For the purpose of control, all operation conditions were kept the same as those of cyclic aging. An FCT test station (EMREL-10A-60W load box, other features are the same as or comparable to that used for MEA1) was utilized for MEA2 operation and characterizations (this test station is denoted as test station #2).

2.2.2. End-of-period diagnosis

The same end-of-period diagnosis procedures were executed for both MEAs. Following the 100 h aging periods, cell operation was halted and the cell polarization, impedance, Tafel plot, H_2 crossover rate and cyclic voltammetry (CV) were evaluated. Aging for the next 100 h period resumed after all characterizations were finished on the next day.

2.2.2.1. Lifetime. To maintain the desired current profile while collecting the lifetime data, a cyclic current step protocol was written to control the load box settings and output. This protocol was based on the Set Protocol.vi from the FCT test station software library, in which users can specify the current settings of the load box under constant current mode, as well as the time delay for each of the current setting after the specification has been reached [9]. At the same time, voltage, current, gas flow rates and temperatures of the running MEA were monitored and recorded via an independent Labview file (Alone LT.vi, also from the FCT software library) with a sampling rate of 120 point h^{-1}. For the constant current aging mode, current was simply adjusted to the set point while the lifetime test was running. In both cases, the aging data collection began when the MEA was re-heated for the next aging period and then lasted 100 h covering the whole aging period. In particular, open circuit voltages (OCV) and voltages at specified current densities were collected and compared at the beginning and end of each aging period.

2.2.2.2. Cell polarization. The cell polarizations were examined in both ascending and descending current control modes shortly after the aging period was ended. The current density range was between 0 and 1.3 A cm^{-2}, with a delay of 30 s at each current setting. Before each of the polarization measurements, a shunt calibration was performed. The shunt resistances were approximately 5.00×10^{-3} Ω for test station #1 and 1.53×10^{-2} Ω for test station #2. High frequency resistances of the cell were measured at all stepwise current levels when polarization data were being taken. Beside that, the independent high frequency resistance control panel (HFR.vi) was executed to validate the resistance of the cell (evaluated by polarization experiments) with a signal magnitude of 7.00×10^{-2} A and frequency of 6000 Hz.

2.2.2.3. Impedance test. Cell impedance tests were implemented using an FCT in-box ac-impedance system at three different current density levels, 0.17, 0.64 and 1.10 A cm^{-2}—representing the kinetic, ohmic and mass transport region of a PEM fuel cell polarization curve. Sinusoidal current waves were emitted through the cell and shunt, with a frequency range of 10,000–0.1 Hz. The magnitude of current wave was also 7.00×10^{-2} A. By examining the voltage drop over the shunt, the complex resistance of the fuel cell electrodes (especially cathode) can be calculated. The Nyquist plots, which are plots of the imaginary resistance versus the real resistance, were generated by the software. From these plots, the values of resistances and capacitances in the PEMFC electrodes (see the equivalent circuit in Fig. 1) R_1, R_2 and C_p were determined.

2.2.2.4. Tafel plot. The Tafel plots of MEA1 and MEA2 were obtained in potentiodynamic mode by a Solartron Analytical 1480 multistat. Channel 1 of the multistat was connected to the positive (red) and negative (black) leads of the fuel cells, with the H_2 electrode acting as both the counter and reference electrodes. The potential of the fuel cell was controlled by the multistat to decrease from OCV to the potential where the current density reached 0.2 A cm^{-2} continuously with a rate of 1 mV s^{-1}. A sampling rate of 100 point s^{-1} was applied. When making the Tafel plot of voltage versus log(current density), the potential of the cell was compensated for by adding the product of current and high frequency resistance. The mass transport corrections for cell potential were not performed. The Tafel test was repeated two times to ensure reproducibility.

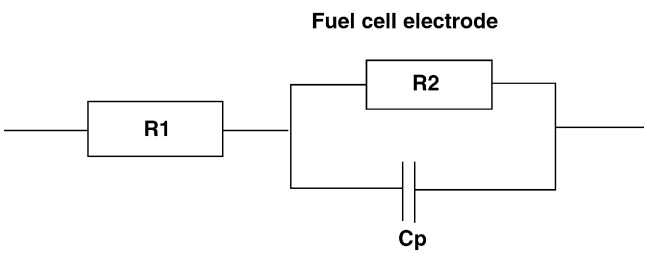

Fig. 1. Schematic of the PEM fuel cell electrode equivalent circuit [9].

2.2.2.5. Hydrogen crossover. The hydrogen crossover rate is an important parameter for determining the permeability of membrane in a fuel cell. If the hydrogen crossover rate from the anode to cathode increases dramatically, it is usually assumed that macroscopic pinholes have formed in the membrane. This would give an indication that the fuel cell is at the end of its useful lifetime. When measuring the hydrogen crossover rate, the cathode gas flow was switched from air to ultrapure nitrogen, with a flow rate of 200 sccm and still having a backpressure of 138 kPa (20 psi). The anode hydrogen flow remained 200 sccm and 138 kPa (20 psi) backpressure. After 40 min of gas equilibration, a potentiostatic assessment at 0.8 V was conducted to measure the current through the fuel cell at 1 point s^{-1} for 5 min. The measured current corresponds to the oxidation of the hydrogen molecules at the cathode side in the presence of platinum catalysts. The anode was taken as the counter/reference electrode, whereas the nitrogen-flowing cathode served as the working electrode. A total of three tests were performed for each end-of-period diagnosis, with the average values recorded.

2.2.2.6. Electrochemical active surface. The evaluation of EAS area was conducted the morning after the hydrogen crossover tests were completed and after the test station was shut down overnight (with the fuel cell connected to the station). The fuel cell fixture had sat for approximately 12 h and cooled to room temperature. There are two reasons for this test procedure: (1) to try to eliminate the adverse effect of hydrogen crossover on CV experiments at high temperatures; (2) to simulate the overnight parking of a passenger vehicle. The EAS areas of both the anode and cathode were estimated by use of a three-cycle-triangle CV. The cathode EAS was first measured by purging H_2 through the anode line (reference/counter electrode) and N_2 through the cathode line (working electrode) with 200 sccm of gas flow and no backpressure for 35 min. After three cathode CV tests were taken, the extension tubing was employed to change the flow path, with 200 sccm of H_2 flowing through cathode and N_2 flowing through anode. In this case, the counter/reference-working electrodes were switched within the fuel cell. Therefore, the leads connecting to the multistat were re-wired, with the black anode lead from the fuel cell joining the red working electrode lead from the multistat. Once again the gases were allowed to flow for 35 min before the CV experiment was started and repeated two times. After anode and cathode CV, both electrodes were purged with N_2 at 200 sccm with zero backpressure for 35 min. By doing so, the CV baselines were obtained and the hydrogen gas left on the cathode when performing the anode CV was able to be discharged, which greatly reduced the chance of cathode catalyst evolution due to the intermediates from the electrochemical reaction of air and residual hydrogen molecules. Then the next aging period was started.

2.2.2.7. Fluoride ion concentration/pH measurements. In order to examine the degree of chemical degradation in the ionomer, the fluoride ion concentrations and the pH values of cathode outlet water were evaluated. The cathode water was collected into an environmental sampling glass jar (pre-cleaned, cap with PTFE lining, VWR.com) during the last 48 h (cyclic) or 12 h (constant) of the aging period, when the cathode venting system was believed to be flushed thoroughly from the previous operation. The jars were washed again before use by deionized water and then isopropyl alcohol for three times, and then blown dry using ultrapure nitrogen gas. A standard solution with fluoride ions was prepared in advance to calibrate the Orion 96-09 fluoride ion combination electrode with low-level total ionic strength adjustment buffer solution (TISABII) added into the standard solution. An Orion 4-star pH/ISE bench top meter was utilized to read out the dc millivolt signal from the fluoride ion combination electrode. The direct calibration method was applied to determine the fluoride ion concentration in the cathode water by measuring the output voltage of the sample solution and comparing with the calibration curve. Meanwhile, pH values of the cathode water were determined using an Orion 520 A pH meter.

3. Results and discussions

3.1. Experimental observations

In this section, the observations and results from the two MEAs aged under cyclic and constant current conditions are summarized and compared. Discussions regarding to the impacts of aging profile on MEA degradations are also presented.

3.1.1. Lifetime data

The voltage profiles of MEA1 in three complete cycles are plotted for each 100 h aging period in Fig. 2. It can be seen that the voltages needed to maintain the specified current output decreased with time, and the voltage profile shifted downward quickly for the last three aging periods. During the last 100 h aging period from 900 to 1000 h, voltage was just above 0.1 V at 1.06 A cm^{-2}, implying that the MEA1 was close to its lifetime if the highest current level had to be reached. This may be the case for vehicles being driven in an uphill road situation. It should be noted that the lifetime of MEA1 seems rather short, compared to the literature values [2–6]. Unfortunately we were not able to obtain the manufacturing details for the commercial MEAs

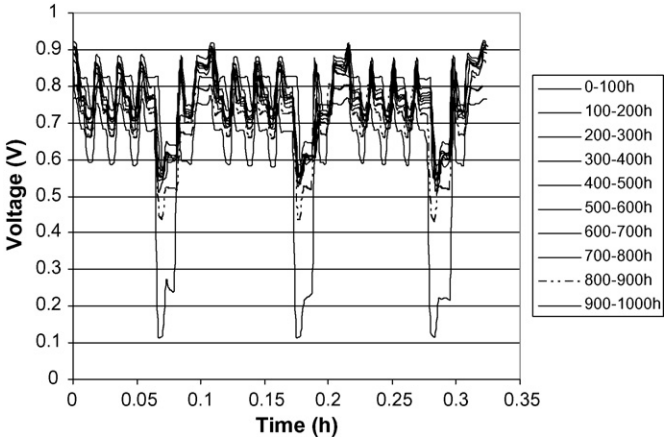

Fig. 2. Comparisons of voltage profile of MEA1 (in three complete cycles) showed lower and lower voltages during the cyclic current aging process.

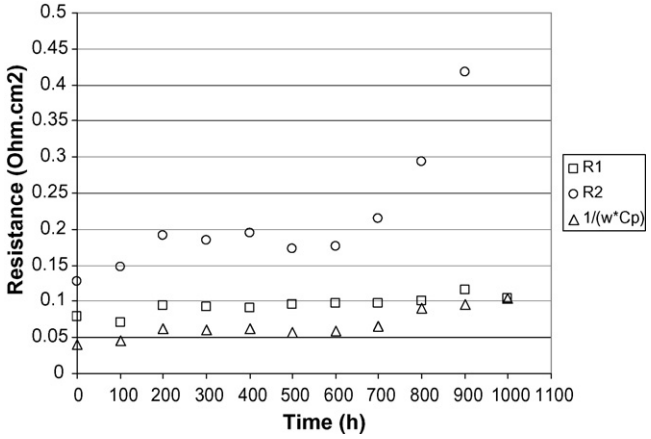

Fig. 3. The low frequency resistance of MEA1, R_2 increased more significantly with time, here $w = 2\pi f$ and f is the frequency at 100 Hz.

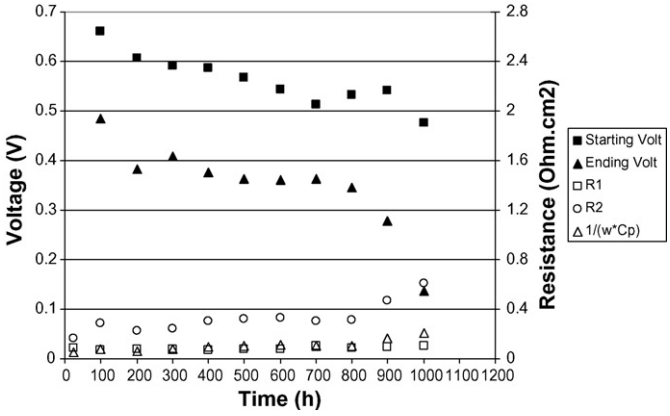

Fig. 4. Cell voltages of MEA2 at 1.06 A cm^{-2} showed continuous decreases at the beginning and end of the 10 aging periods under constant current mode. Similarly, R_2 increased with time.

that we tested in our experiments. Nevertheless, the chances of experimental artifacts were minimized when we characterized the two MEAs, by carefully monitoring the operations of the FCT test stations with regard to temperature, pressure, gas flow and humidification control.

Fig. 3 shows the values of high frequency resistance R_1, electrode resistance R_2 (the result of subtracting R_1 from the real resistance at low frequency) and the electrolyte–catalyst differential capacitance C_p of MEA1 at an intermediate current density. It reveals that high frequency resistance R_1 and capacitance C_p had almost constant values throughout the entire aging process. The electrode resistance at low frequency, R_2, increased more significantly by approximately 100% at 900 h. The value of R_2 could not be estimated at the end of 900–1000 h aging period due to the unsteady current during the impedance measurement.

According to Lefebvre et al., R_2 can be considered as the specific combination of electronic resistance and ionic resistance from the membrane phase in the catalyst layer [10]. The increase of R_2 along with time (Fig. 3) indicates that the carbon support beneath the platinum particles might have been corroded or the recast ionomer at the electrolyte–catalyst interface had degraded, or both. More details in this regard will be discussed later in conjunction with the cathode water analysis.

Fig. 4 illustrates the decay of voltages at the constant current density of 1.06 A cm^{-2} for MEA2. The voltages were recorded and averaged at the beginning and end of 10 constant aging periods. Once again, the voltage decay was observed to occur very rapidly, with estimated rates of $-160\,\mu V\,h^{-1}$ for voltages at the beginning of aging periods and $-255\,\mu V\,h^{-1}$ at the end. The rates were considerably higher than those reported in the literature (~ -21 to $-127\,\mu V\,h^{-1}$ [2]). In addition, there was continuous decrease of voltages within each 100 h aging period as shown in Fig. 4 (by comparing the voltages vertically at the same time nodes), mainly due to the mass transport limitations existent on the cathode side. It was observed that the voltage continued to decrease for certain amount of time when the constant current operation resumed after the end-of-period diagnosis, and then reached a stable value for the rest of the aging period. The reason behind this phenomenon may be related to the slow competition among product water, humidification vapor and cathode water discharge. The cathode of MEA2 went through stages of initial dryness, water accumulation and final saturation at 1.06 A cm^{-2}. Since we were utilizing the standard 5 cm^2 test fixture and Teflon-coated fiber glass sealing gaskets, it may be that the commercial MEAs (supplied with GDL) did not possess good water expelling properties. Similar to MEA1 under cyclic aging conditions, the electrode resistance R_2 almost doubled at 1000 h. The electrolyte–catalyst differential capacitance C_p decreased (as $1/(w^* C_p)$ increased), indicating less charges may be stored in the carbon–catalyst–ionomer three-phase region.

3.1.2. Hydrogen crossover rate and open circuit voltage

The trends of OCVs at the beginning and end of aging periods as well as the hydrogen crossover rates as a function of time are shown in Fig. 5 for the cyclic current mode and Fig. 6 for the constant current mode. The OCVs of cyclically aged MEA1 remained at approximately 0.9 V until 500 h, when there were small differences between the values of OCVs at the beginning and end of aging periods. After 600 h, bigger discrepancies began to exist due to aging and the OCV decreased almost linearly. At the end of 900–1000 h aging period, the OCV was as low as 0.28 V. The decrease of OCV can usually be related to

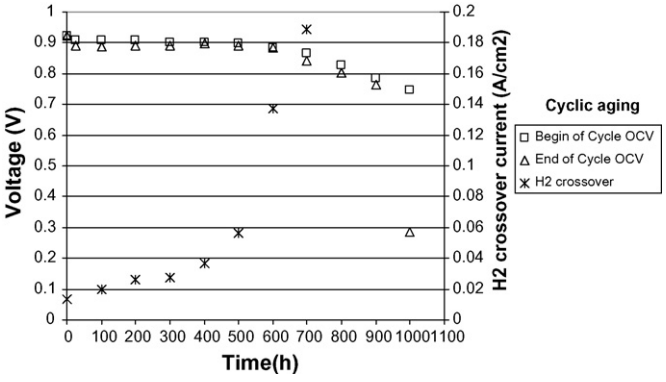

Fig. 5. Decay of OCVs at the beginning and end of the 100 h aging periods complied well with the trend of hydrogen crossover rate for MEA1 under cyclic current mode.

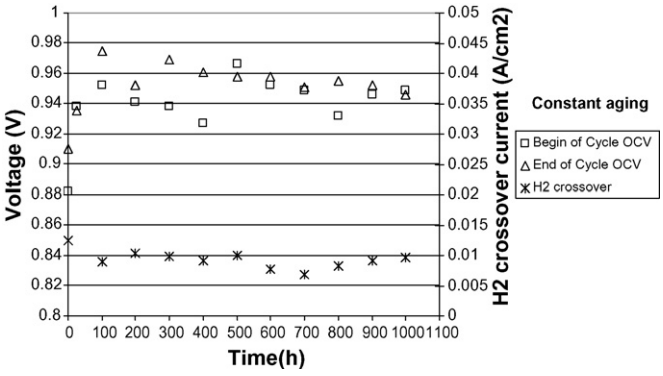

Fig. 6. The OCVs of MEA2 at the beginning and end of the 100 h aging periods and the hydrogen crossover rate remained relatively constant under constant current mode (1.06 A cm^{-2}).

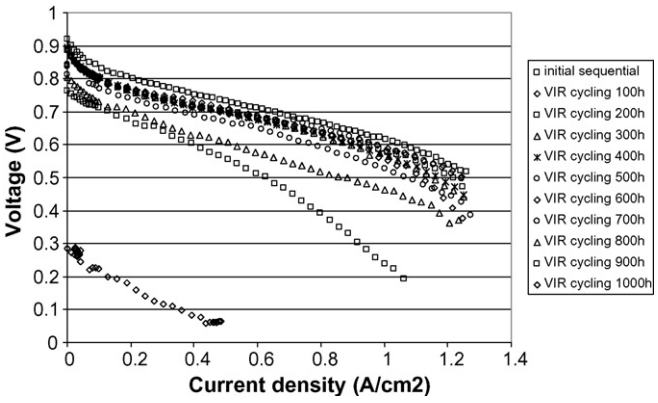

Fig. 7. The polarization curves of MEA1 shifted downward during the cyclic current aging process mainly because of the lowering of OCV caused by hydrogen crossover.

the loss of reactants (especially the fuel) or crossover of fuel to the cathode in the fuel cell system. In our case, the OCV decay was in good accordance with the results of hydrogen crossover measurement. The hydrogen crossover rate rose considerably high after 500 h and the potentiostat was not able to hold the fuel cell at 0.8 V for a certain amount of time without exceeding the instrument limit between 800 and 1000 h. Thus, no data points were plotted in Fig. 5 at these times. A reasonable explanation for the dramatic leap of hydrogen crossover rate was formation of pinholes in the N112 membrane after 500 h of current cycling. Although it is difficult to attribute the pinhole formation to sole mechanical or chemical degradations in the membrane, the outcome of the degradations was permanently changing the membrane by forming macroscopic holes in it. Otherwise the hydrogen crossover rate would not be as high as 0.3–0.95 A cm^{-2}, assuming under normal circumstances the hydrogen molecules that migrated from anode to cathode came all from dissolved hydrogen.

Our results from accelerated cyclic current aging suggested that the resistance of membranes to chemical and mechanical degradations is very important to sustain the fuel cell through various operation conditions and to last long enough in automotive transportation. Therefore, the durability of the membrane materials has to taken into account when developing the next generation proton exchange membranes, particularly the ability of the membranes to endure not only the attack of hydrogen peroxide radicals, but also hydrothermal mechanical stress. This may require the membranes to be a comprehensive product of tailored properties such as thickness, proton conductivity, mechanical strength/modulus, swelling behavior and so on.

On the other hand, the OCVs of constant-current aged MEA2 fell into the 0.92–0.98 V region during the entire 1000 h of aging. The hydrogen crossover rate fluctuated around 0.01 A cm^{-2}. No physical holes should have appeared in the membrane; otherwise considerable hydrogen crossover would have caused the OCVs to drop to a large extent. This may be due to the fact that the membrane was wet for most of the time (operated at constant current density of 1.06 A cm^{-2}). The membrane was expected to have less mechanical degradations while the cyclic stresses due to dry–wet cycles did not exist in the MEA2 under constant current operation.

3.1.3. Polarization curves

The polarization curves of MEA1 under cyclic current aging mode are shown in Fig. 7. When one examines the kinetic, ohmic and mass transport regions of the polarization curves, it is clearly illustrated that the most significant degradation that occurred to MEA1 was the lowering of the OCV, caused by the large amount of hydrogen crossover. The slopes of the curves at the ohmic region were very similar until 900 h. The polarization curve at the end of 1000 h aging was almost a straight line at very low current and voltage levels, indicating that MEA1 was approaching the end of its lifetime.

The polarization curves of MEA2 aged under constant current are plotted in Fig. 8. They demonstrate a very different trend compared to those of MEA1. Being consistent with the OCV result, the polarization curves converged to the approximate value of ~0.96 V at zero current density. There are larger discrepancies at the ohmic region of the polarization curves for MEA2, though the values of electrode resistances and capacitances (R_1, R_2, C_p measured from the impedance tests) did not change much through the aging process (see Fig. 4). This may be attributed to the influence of mass transport on system characteristics. As mentioned before, the MEAs that we investigated in this study did not possess satisfactory long-term

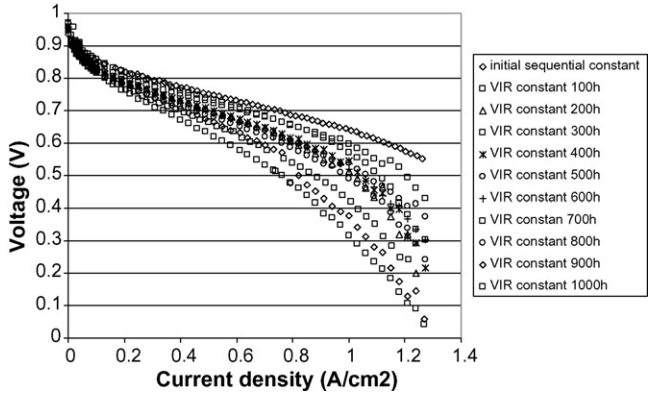

Fig. 8. Comparisons of the polarization curves of MEA2 illustrated major degradations in the mass transport region during the constant current aging process.

water management properties. The situation may have become so bad that the mass transport overpotential of the MEA2 began to decrease the cell voltage at a lower current density. However, the mass transport degradations that occurred to MEA2 were partially reversible, as we performed the end-of-period diagnosis with lower current densities. By the time the impedance measurements were taken, the degree of water saturation on the cathode side of MEA2 may have already changed from that when MEA2 was actually aged at the current density of 1.06 A cm^{-2}.

The reversibility of mass transport limitation could also help explain why the polarization curves for MEA2 did not shift downstream in a straight order of 100, 200, 300, . . ., 1000 h. The fuel cell characterizations themselves may control the MEA to be under certain conditions, which could perhaps alter the state of the MEA itself. As a result, the long-term characteristics of fuel cell MEAs should be judged relatively, because the results are affected by the operation history of the MEAs by various instruments. Therefore, there is a need to establish a standard protocol for PEMFC durability diagnosis, simply to make the test results obtained from different agencies comparable.

3.1.4. Tafel plots

Fig. 9 shows the Tafel plots of the MEA1 from break-in to the last aging period. The Tafel plots can be divided into two groups with the division marked by a large shift-down between 600 and 700 h, corresponding to the large increase of hydrogen crossover rate. This further demonstrates the change in the fuel cell at that time, most likely due to pinhole formation in the membrane. Although an attempt was made to extract electrochemical kinetic parameters from the Tafel plots, no reasonable values for Tafel slope b and exchange current density i_0 were successfully obtained. From Fig. 9, it is discernable that the voltage–log(i) plots formed nearly horizontal lines till 10^{-4} to 10^{-3} A cm^{-2} of current densities and then curled up continuously at higher current densities. There were no distinct linear regions from these curves, which resulted in great difficulty and uncertainty in determining the values of Tafel slopes and extrapolating the curves to intercept the highest horizontal lines at equilibrium. Wang et al. at Argonne National Laboratories (ANL) employed a rotating ring-disk electrode (RDE) apparatus to evaluate the oxygen reduction reaction (ORR) kinetics [11]. By applying the RDE technique, a well controlled mass transfer environment was provided for the electrochemical reactions to occur in a much more delicate manner than that manipulated by a fuel cell test station. Consequently, the mass transport effect on potentiodynamic cell operation was minimized and the current density of the fuel cell can go down to as low as 10^{-11} A cm^{-2}. The ANL effort showed that the exchange current density for ORR at the platinum/carbon/Nafion interface at 90 °C was about 3.1×10^{-9} A cm^{-2}, a number that is beyond the lowest limits of the Tafel plots we obtained by simply connecting the fuel cell test station with the potentiostat. Therefore, despite the fact that the current state-of-the-art fuel cell test station could perform the bulk of the MEA characterizations, development of more accurate mass transport control is required as to improve the accuracy of electrochemical kinetics measurements.

It can be seen in Fig. 10 that the Tafel plots for MEA2 under constant aging mode were almost identical except the one taken right after break-in period. These results substantiated the reversibility of mass transport-induced degradations in fuel cell performance. Again, when the Tafel plots were acquired, the water content in the MEA2 cathode further decreased. Air could flow better and reach the reaction sites much easier after the flooding problem was resolved at the cathode. The Tafel plots did not display significant degradations even at 1000 h with current densities ranging between 0 and 0.2 A cm^{-2}. Although the aging experiment was terminated, it is reasonable to expect that the lifetime of MEA2 could be well above 1000 h. The mass transport issues can be mitigated by frequently drying out the MEA2. Based upon above observations, we found out that the current output profile of the fuel cell has had a strong impact on its degradation mechanisms, long-term performance and ultimately, the lifetime. Hence, simplistic testing and verification of new materials (especially membranes) after break-in via polarization curve measurements may not be sufficient to support the full validity of those materials to be utilized as fuel cell components. Systematic evaluation with respect to various operation conditions is preferred.

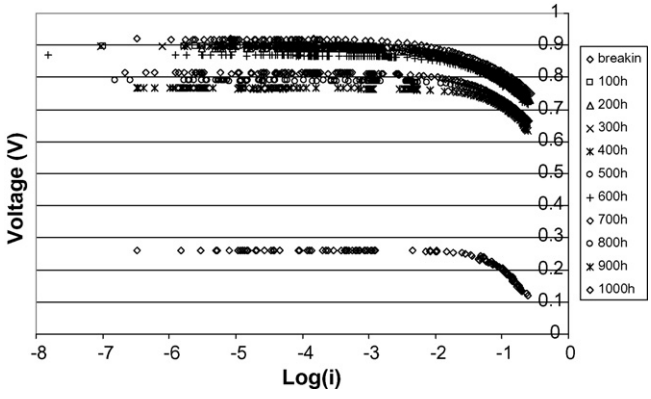

Fig. 9. Tafel plots of MEA1 operated using FCT test station #1 had lower and lower voltages at current densities up to 0.2 A cm^{-2} during the cyclic current aging process.

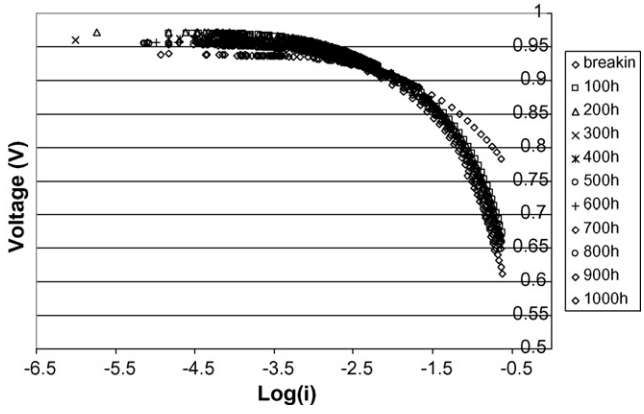

Fig. 10. Tafel plots of MEA2 were almost identical except the one taken after break-in during the 1000 h of constant current aging process.

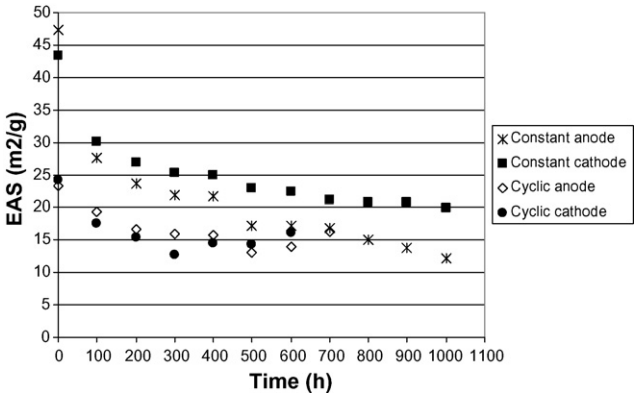

Fig. 11. The changes of EAS areas as a function of time were shown for both anode and cathode of MEA1 and MEA2.

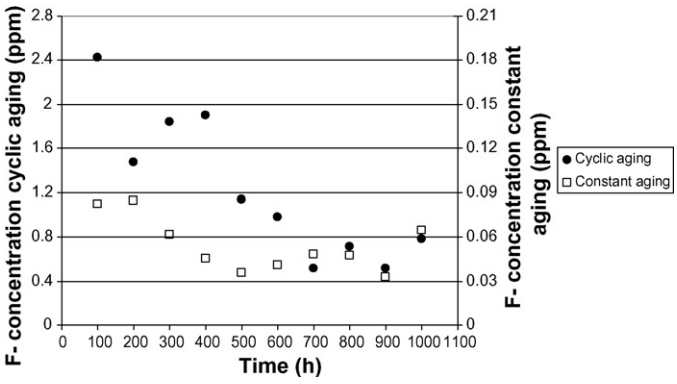

Fig. 12. The fluoride ion concentrations in cathode outlet water were measured for MEA1 under cyclic aging conditions and MEA2 under constant aging conditions. The fluoride ion release rate was about 30-fold larger for MEA1 than that of MEA2.

3.1.5. EAS trends for both electrodes

Fig. 11 illustrates both of the anode and cathode EAS areas against time for MEA1 and ME2. The EAS could not be measured by CV after 600–700 h of aging under cyclic current aging conditions due to large amount of hydrogen crossover. In spite of the fact that the two MEAs were supposed to be manufactured the same way, the initial EAS areas of MEA2 were almost twice as those of MEA1, which implies that the current MEA manufacturing technique may still have limitations in terms of product consistency. Nevertheless, the EAS of both MEAs showed similar trends of exponential-like decay, while the constant current-aged MEA2 lost its EAS at a faster speed. Based on our current understanding, the decrease of EAS will have a significant impact on the fuel cell performance. For most of the cases, the output current produced from an energy device is quantified in the form of current density, defined as the current divided by the active surface area of the device. In the case of fuel cells, the current density is calculated using the nominal MEA area (such as 5 cm^2), i.e., the area of a common region shared by the fuel cell membrane, catalyst layer and gas diffusion layer. Yet, the current drawn from a fuel cell system is actually generated at the electrochemical active sites. If less EAS (hence less energy density) is available for the electrochemical reactions to take place while the output current density is still regulated as the same by the electronic load box, one can imagine that the voltage needed to drive the fuel cell has to be lower according to the polarization nature of the fuel cell. In order to reflect this process, a mathematical manipulation was invented by use of a term named "local current density", which is the outcome of nominal current density and percentage of residue EAS on the fuel cell electrodes. The influence of EAS on cell performance has been taken into account during our phenomenological durability modeling, as further described in Section 3.2.

3.1.6. Fluoride ion concentration and pH curves

The trends of fluoride ion concentration in the cathode exhaust water were compared for MEA1 and MEA2 in Fig. 12. The fluoride ion concentrations decreased along with time, as opposed to the results reported by Xie et al. [6]. The probability of artifacts from contamination of the water sample was small, because there was enough time including MEA break-in period to wash away any residue fluoride ions left in the fuel cell testing system before the first water sample was collected. If we assume the fluoride ion release rate from the MEA was proportional to the fluoride ion concentration in the cathode outlet water, it is very likely that the fluoride ions came from the decomposition products of the recast ionomer in the catalyst layer (corresponding to the increase of R_2) and/or the membrane. The trends of the fluoride ion concentration in Fig. 12 resembled the solution to first order reaction kinetics equation:

$$\frac{dM}{dt} = -kM \quad (1)$$

where M is the mass of the recast ionomer/membrane (Nafion) present and k is the rate constant for decomposition. This observation coincides with the remarks given in Ref. [14] that the kinetics of Nafion membrane degradation in Fenton's reagent can be represented by the expression of Ref. [12]:

$$-\log(\%\,\text{degradation}) = kt \quad (2)$$

It also appears that the fluoride ion concentrations from MEA1 under cyclic current aging conditions were about 30-fold higher (the water generated by the ORR at the cathode is 1/3 of that under constant current mode) than those from MEA2 under constant current operation. Although more experiments need to be performed to confirm our observation, the fact of early membrane failure with cyclic current output implies that there might be strong interactions between the chemical and mechanical degradations of ionomers. Hygromechanical stress may accelerate the chemical decomposition of Nafion, most likely, the dissolution of recast Nafion ionomer in the catalyst layer, referring to the suggestions by Xie et al. [6] and LaConti et al. [12].

The detailed study of Nafion membrane decomposition in Fenton's reagent or in the fuel cell environment has been carried out in companies including Dupont, General Motor (GM), United Technologies Corporation (UTC) fuel cells and 3 M. The chemical degradation mechanisms were investigated based on the method of model compounds and some basic agreements have been reached. It is usually considered that the peroxides and their radicals attack the carboxylate end groups of Nafion,

$$(CF_2)_n\text{-}CO_2H + H_2O_2 \rightarrow (CF_2)_n CO_2^{\cdot} + {\cdot}OH$$

$$(CF_2)_n\text{-}CO_2^{\cdot} + {\cdot}OH \rightarrow (CF_2)_{n-1} CF_2OH + CO_2\uparrow$$

$$(CF_2)_{n-1}\text{-}CF_2OH \rightarrow (CF_2)_{n-1}COF + HF$$

$$(CF_2)_{n-1}\text{-}COF + H_2O \rightarrow (CF_2)_{n-1}CO_2H + HF$$

Scheme 1. The proposed chemical degradation mechanism of Nafion, which involves attacks of carboxylate end group by peroxide and sequential propagation along the main chain.

which release carbon dioxide (CO_2), hydroxyl radical ($OH^{\bullet}$) and hypofluoric acid (HF) and form new carboxylate groups at the chain ends. By repeating the process, the attack propagates along the main chain of the polymer (refer to Scheme 1 [13]). Consequently, one could expect variations with respect to the pH values of cathode exhaust water. Fig. 13 illustrates the changes of pH as a function of time for both MEA1 and MEA2. Surprisingly, the pH values showed opposite trends for cyclic and constant current mode. The pH of cathode water collected under cyclic aging conditions decreased first, and then increased. It can be speculated that the membrane degradation had taken place more thoroughly with cyclic current profile, where a certain amount of hypofluoric acid was generated. Hence, the pH value decreased. As the chemical degradation of Nafion slowed down because of the reduction in mass of the available ionomer, less HF acid was produced and the pH increased. Meanwhile, for the case of constant current aged membrane, the peroxide attack might have been terminated at the earlier steps, which gives off $OH^{\bullet}$ radicals as the side product. This would lead to a higher value of pH, as evidenced in Fig. 13. Similarly, when less ionomers were left in the fuel cell, the release of hydroxyl radicals was lowered, raising the pH values.

3.2. PEMFC durability modeling

The semi-empirical phenomenological durability modeling for PEMFCs under both cyclic and constant aging conditions was attempted to incorporate observed aging phenomena and describe the cell performance at different time periods.

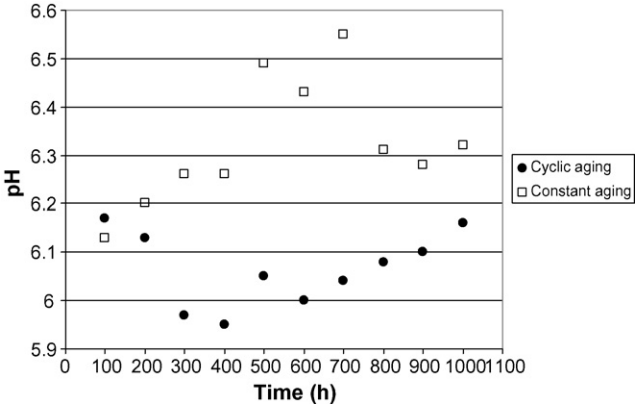

Fig. 13. The pH values of the cathode outlet water demonstrated opposite trends for MEA1 under cyclic aging condition and MEA2 under constant aging condition.

3.2.1. Modeling principles

The semi-empirical equation that comprises the core of the phenomenological durability model is as follows [14]:

$$V = E_r - \frac{RT}{2F}\ln\frac{a_{H_2O}}{a_{H_2}a_{O_2}^{1/2}} - iR_H - A\ln\frac{i}{i_0} + B\ln\left(1-\frac{i}{i_l}\right) \quad (3)$$

where E_r is the cell reversible potential and equal to 1.18 V at the cell temperature of 80 °C [14], a_{H_2}, a_{H_2O} and a_{O_2} are the chemical activities of the fuel, oxygen and product water, R_H is the high frequency resistance of the fuel cell measured simultaneously with the polarization curves, A and B are constants and both equal to as $RT/n\alpha F$. Here R is the gas constant, T the absolute cell temperature, n the number of electrons transferred per electrochemical act, α the charge transfer coefficient and F is the Faraday's constant. The symbol of i_0 is the exchange current density that is assumed to be a constant during the entire aging process. Most importantly, i is the mathematical "local current density" that is "modulated" on the membrane–catalyst interface to achieve the nominal output of current density and can be calculated based upon the nominal/apparent current density i_{app}, the internal current density due to hydrogen crossover i_n and the percentage of residue catalyst surface area p_{eas} as

$$i = \frac{i_{app} + i_n}{p_{eas}} \quad (4)$$

Similarly, i_l is a function of the limiting apparent current density i_{l0} (the current density at which cell voltage goes to zero) and can be calculated by $i = (i_{l0} + i_n)/p_{eas}$.

Having the main equation set up, the model parameters including R, i_n, p_{eas} and i_{10} were then implemented into the semi-empirical equation with values corresponding to 11 time nodes, 0, 100, 200, 300, . . ., 1000 h. The exchange current density i_0 was utilized as the sole adjustment parameter during the modeling process. The voltage decays at several current densities under constant current mode and in three aging cycles under cyclic current mode were computed. The cell polarization curves at 11 time nodes were assessed and compared with the experimental results.

3.2.2. Modeling results

Fig. 14 presents the modeling and experimental voltage results for MEA2 at current densities of 0.2, 0.7 and 1.06 A cm^{-2}. It can be seen that the "model-predicted" trends provided very good fits to the experimental data. In particular, for voltages at 1.06 A cm^{-2}, the voltage curve fell in between the actual voltages measured at the beginning and end of the 10 aging periods. This is what we have expected, since the values of the model parameters were obtained when the water content of the MEA2 already deviated from that during the constant current operation and ranged between the numbers at the driest and wettest states.

The results in Fig. 15 demonstrate that the phenomenological durability model can successfully generate the polarization curves for aged MEAs at different time periods. The calculated polarization curves shifted downward and the current density at

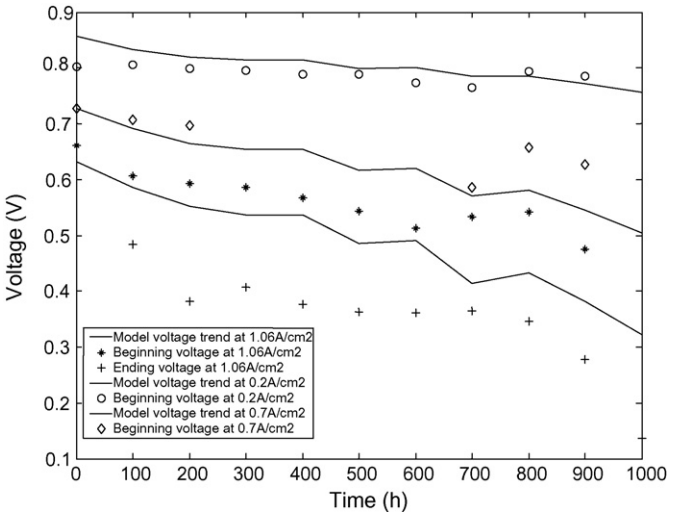

Fig. 14. The model predicted and experimental voltage trends for MEA2 at 0.2, 0.7 and 1.06 A cm^{-2} under constant aging conditions.

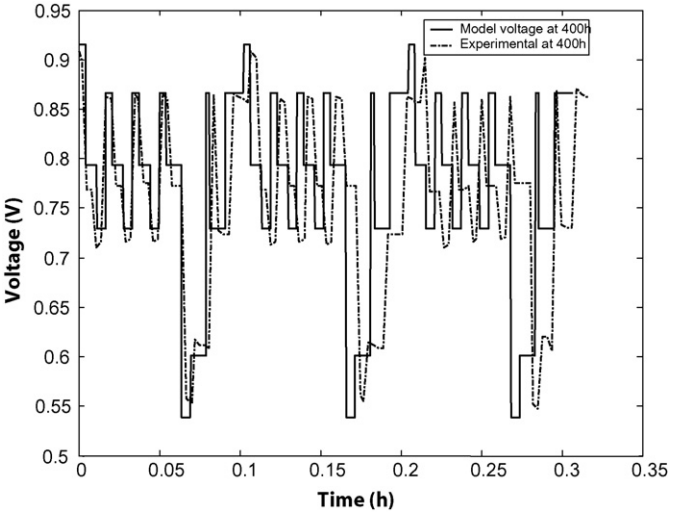

Fig. 16. The model predicted and experimental cyclic voltage profiles for MEA1 at 400 h.

which the power curves reached their peak values was lowered in a similar fashion as the experimental results. The maximum power output decreased by approximately 10%, which is a good indication of the deterioration in the fuel cell. This type of information is quite useful when evaluating the extent of degradations in fuel cells, but certainly time-dependent constitutive relations for fuel cell components need to be incorporated into the durability model as to bring the model with more predictive power.

The model predicted and experimental cyclic voltage profiles for MEA1 at 400 h were illustrated in Fig. 16. The experimental voltage profile was found to have larger and larger phase lag behind the model predicted profile. The reason behind this may be due to the "ramp times" for the current to change from one setting to another. It took some time (although may be very short) for the fuel cell system to complete current step changes, especially the more dramatic ones such as step 14 to step 15 in Table 1.

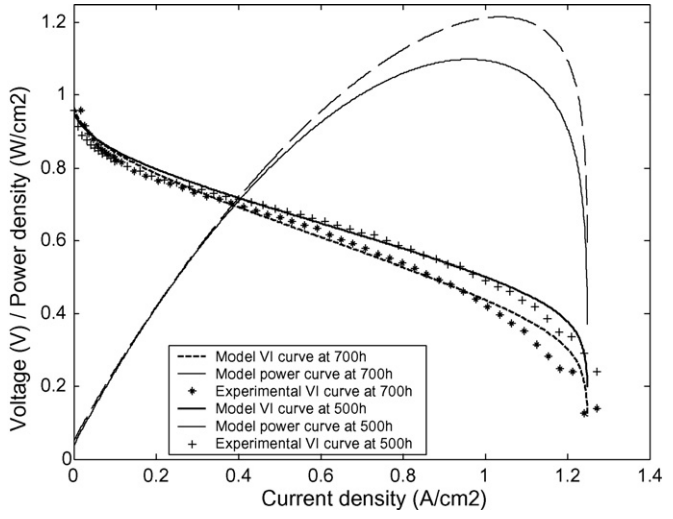

Fig. 15. The model predicted and experimental polarization curves for MEA2 at 500 and 700 h under constant aging conditions.

Once the designated current level was reached, the fixed plateau time when the current stayed at the set point began to elapse till the onset of next segment. This lagging behind due to extra "ramp time" further accumulated down the road, creating more and more phase differences. It should be noted here that the phase lag between model predicted and experimental voltage profile is a reflection of the nature of our phenomenological model. The phenomenological model is a steady-state model that computes the performances of the PEM fuel cell only at specified time nodes. A transient model is required in order for the model to capture the dynamic behavior of a fuel cell under current step changes. In automotive applications, power electronics and control units should be designed properly to help mitigate the phase lag.

4. Conclusions

In this article, the long-term durability of hydrogen–air proton exchange membrane fuel cells (PEMFCs) was investigated under both cyclic and constant current conditions for 1000 h using the same type of MEAs. The end-of-period diagnosis including cell polarization, impedance spectrum, Tafel plot, hydrogen crossover rate as well as electrochemical active surface area was performed at a regular basis. It was demonstrated that hydrogen crossover was the most dominant degradation for cyclic current aging after 500–600 h and the MEA1 reached its lifetime after 1000 h of operation. Mass transport limitations were identified as the major degradation source of the MEA2 under constant current conditions. The degradation in performance of MEA2 was partially reversible when cathode flooding was resolved after the cell undergone the series of end-of-period characterizations. A semi-empirical phenomenological durability model was successfully established to incorporate the aging observations and describe the cell performance along with time. The results illustrated the demand for standard fuel cell durability test protocol and membrane pinhole reduction study.

Acknowledgements

The authors would like to express its sincere gratitude to the Macromolecules and Interfaces Institute (MII) at Virginia Tech for its support for the lead author as an MII Research Frontiers Fellow. They highly appreciate the help from Dr. Mike Ellis at the Mechanical Engineering Department of Virginia Tech for the access of fuel cell test stations and potentiostat. They also thank Dr. Yeh-hung Lai, Kim Greenberg and Michael Budinski at General Motors Fuel Cell Activities for their efforts in providing the cyclic current aging spectrum and inspecting the aged MEAs. Finally the valuable discussions with Dr. Michael Hickner of Sandia National Laboratories are acknowledged.

References

[1] D.O. Energy (Ed.), Basic Research Needs for the Hydrogen Economy, report of the basic energy science workshop on hydrogen production, storage and use prepared by Argonne National Labrotaries, Rockville, Maryland, 2003, pp. 53–60.
[2] D.P. Wiklinson, J. St-Pierre, Chapter 47: durability, in: W. Wielstich, H.A. Gasteiger, A. Lamm (Eds.), Handbook of Fuel Cells—Fundamentals, Technology, Applications, John Wiley & Sons, Ltd., 2003.
[3] V. Stanic, J. Braun, M. Hoberecht, Durability of membrane electrode assemblies (MEAs) in PEM fuel cells operated on pure hydrogen and oxygen, in: Proceedings of the First International Energy Conversion Engineering Conference, Portsmouth, Virginia, 2003.
[4] J. St-Pierre, N. Jia, Successful demonstration of ballard PEMFCS for space shuttle applications, J. New Mater. Electrochem. Syst. 5 (2002) 263–271.
[5] J. St-Pierre, et al., Relationships between water management, contamination and lifetime degradation in PEFC, J. New Mater. Electrochem. Syst. 3 (2000) 99–106.
[6] J. Xie, et al., Durability of PEFCs at high humidity conditions, J. Electrochem. Soc. 152 (1) (2005) A104–A113.
[7] fuelcellstore.com, 5L HP-A MEA, item # 590514.
[8] Airgas, hydrogen: UPH-300; air: AIR-300; nitrogen: UPN-300.
[9] D. McMurry, C. DeRouin, Fuel Cell Technologies Fuel Cell Test Station Software Manual, Albuquerque, 2003.
[10] M.C. Lefebvre, R.B. Martin, P.G. Pickup, Characterization of ionic conductivity profiles within proton exchange membrane fuel cell gas diffusion electrode by impedance spectroscopy, Electrochem. Solid-State Lett. 2 (6) (1999) 259–261.
[11] X. Wang, D. Myers, R. Kumar, Non-Precious Metal Electrocatalysts, Argonne National Laboratory, 2005.
[12] A.B. LaConti, M. Hamdan, R.C. McDonald, Chapter 49: mechanisms of membrane degradation, in: W. Wielstich, H.A. Gasteiger, A. Lamm (Eds.), Handbook of Fuel Cells—Fundamentals, Technology, Applications, John Wiley & Sons, Ltd., 2003.
[13] S. Hamrock, New membranes for PEM fuel cells, 3M Fuel Cell Components Program, 2005.
[14] J. Larminie, A. Dicks, Fuel Cell System Explained, 1st ed., John Wiley & Sons, 2000.